Molybdenum−Iron−Sulfur Clusters of Nuclearities Eight and Sixteen, Including a Topological Analogue of the P-Cluster of Nitrogenase

Frank Osterloh, Catalina Achim, and R. H. Holm*

Department of Chemistry and Chemical Biology, Harvard University, Cambridge, Massachusetts 02138

Received June 8, 2000

Transformations of the edge-bridged double cubane cluster $[(Cl_4cat)_2(Et_3P)_2Mo_2Fe_6S_8(PEt_3)_4]$ (**1**) under reducing conditions have been investigated as synthetic approaches to the clusters of nitrogenase. Cluster **1** is a versatile precursor to different Mo−Fe−S cluster types. The reaction system **1**/$K(C_{14}H_{10})$ in THF yields the reduced cluster $[(Cl_4cat)_2(Et_3P)_2Mo_2Fe_6S_8(PEt_3)_4]^{1-}$ (**2**), which as its crystalline Et_4N^+ salt retains the edge-bridged structure of **1**. X-ray structural and Mössbauer spectroscopic results indicate an unsymmetrical electron distribution with localized $[MoFe_3S_4]^{2+,1+}$ cubane-type units. The system **1**/2$K(C_{14}H_{10})$/2HS^- in THF/acetonitrile affords $[(Cl_4cat)_4(Et_3P)_4Mo_4Fe_{12}S_{20}K_3(DMF)]^{5-}$ (**3**), whose structure was determined as the Ph_3PMe^+ salt. The cluster consists of two isostructural $Mo_2Fe_6S_9$ fragments connected by two μ_2-S bridges. Three potassium ions are bound between the two fragments. In each fragment, the iron atoms are present in tetrahedral FeS_4 and the molybdenum atoms in octahedral MoO_2PS_3 coordination units, and two $MoFe_3(\mu_3\text{-}S)_3$ cuboidal units are bridged by a common μ_6-S atom. The fragments have idealized mirror symmetry and are isostructural with two of the fragments present in the previously reported high-nuclearity cluster $[(Cl_4cat)_6(Et_3P)_6Mo_6Fe_{20}S_{30}]^{8-}$ (**4**) (Osterloh, F.; Sanakis, Y.; Staples, R. J.; Münck, E.; Holm, R. H. *Angew. Chem., Int. Ed. Engl.* **1999**, *38*, 2066). On the basis of overall shape, atom connectivities, and metric features, the $Mo_2Fe_6S_9$ fragment is a topological analogue of the P-cluster of nitrogenase in the P^N (reduced) state. A third cluster type, formed as a minor byproduct in the reaction system leading to **2**, was crystallographically identified as $[(Cl_4cat)_2(Et_3P)_2Mo_2Fe_6S_8(PEt_3)_4]^{4-}$, whose core is made up of two $MoFe_3(\mu_3\text{-}S)_3$ cuboidal units bridged by two μ_2-S atoms and connected by a direct Fe−Fe bond. Full structural details and the redox properties of **2** and **3** are reported.

Introduction

The two polynuclear centers of nitrogenase, which have been defined by protein crystallography[1−3] and are schematically depicted in Figure 1, represent a unique challenge in cluster synthesis. Certain fragments of these clusters have been achieved in addition to the well-known cubane-type Fe_4S_4 unit, which is part of the P-cluster.[2,3] The cuboidal $Fe_4(\mu_3\text{-}S)_3$ fragment, present in FeMoco and the P^{OX} state of the P-cluster, occurs in $[MFe_4S_6(PEt_3)_4L]$ ($L = Cl^-$, RS^-)[4,5] and in the Roussin black anion $[Fe_4S_3(NO)_7]^{1-}$.[6−8] Cuboidal $MoFe_3(\mu_3\text{-}S)_3$ units similar to that in FeMoco have been stabilized in tetranuclear clusters containing carbonyl and phosphine ligands at the iron sites.[9,10] While these clusters contain nonphysiological iron ligands and attendant stabilization of oxidation levels possibly lower than those accessible in nitrogenase, it is a matter of some interest that native cluster fragment topologies have been achieved in these reduced molecules. In this context, we also note that the bicapped trigonal prismatic metal topology of idealized D_{3h} symmetry in FeMoco has been realized in the strongly reduced clusters $[Ni_8S(SBu^t)_9]^{1-}$ [11] and $[Co_8(NPh)_9(PPh_3)_2]^{4-}$.[12] Here, strong metal−metal bonding in both clusters and in the former

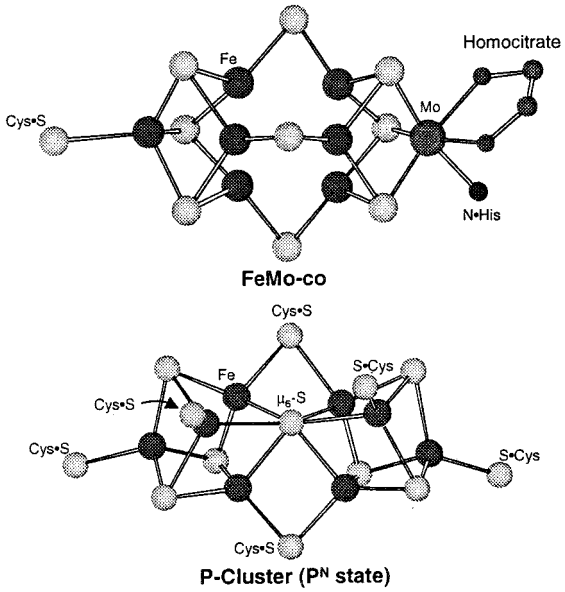

Figure 1. Schematic structures of the clusters of nitrogenase: iron-molybdenum cofactor (FeMoco) and the reduced P-cluster (P^N state).[3]

(1) Chan, M. K.; Kim, J.; Rees, D. C. *Science* **1993**, *260*, 792−794.
(2) Peters, J. W.; Stowell, M. H. B.; Soltis, S. M.; Finnegan, M. G.; Johnson, M. K.; Rees, D. C. *Biochemistry* **1997**, *36*, 1181−1187.
(3) Mayer, S. M.; Lawson, D. M.; Gormal, C. A.; Roe, S. M.; Smith, B. E. *J. Mol. Biol.* **1999**, *292*, 871−891.
(4) Nordlander, E.; Lee, S. C.; Cen, W.; Wu, Z. Y.; Natoli, C. R.; Di Cicco, A.; Filipponi, A.; Hedman, B.; Hodgson, K. O.; Holm, R. H. *J. Am. Chem. Soc.* **1993**, *115*, 5549−5558.
(5) Cen, W.; MacDonnell, F. M.; Scott, M. J.; Holm, R. H. *Inorg. Chem.* **1994**, *33*, 5809−5818.
(6) Chu, C. T. W.; Dahl, L. F. *Inorg. Chem.* **1977**, *16*, 3245−3251.
(7) Scott, M. J.; Holm, R. H. *Angew. Chem., Int. Ed. Engl.* **1993**, *32*, 564−566.
(8) Goh, C.; Holm, R. H. *Inorg. Chim. Acta* **1998**, *270*, 46−54.
(9) Tyson, M. A.; Coucouvanis, D. *Inorg. Chem.* **1997**, *36*, 3808−3809.
(10) Han, J.; Beck, K.; Ockwig, N.; Coucouvanis, D. *J. Am. Chem. Soc.* **1999**, *121*, 10448−10449.

10.1021/ic000617h CCC: $20.00
Published on Web 12/09/2000

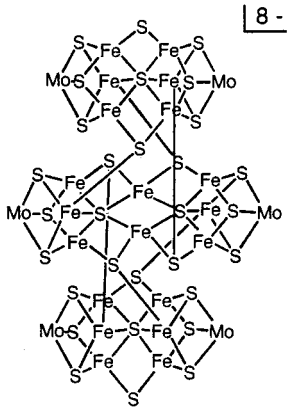

Figure 2. Schematic core structure of centrosymmetric $[(Cl_4cat)_6(Et_3P)_6Mo_6Fe_{20}S_{30}]^{8-}$ showing atom connectivities.[20] All iron atoms are in tetrahedral FeS_4 sites; terminal ligands at 6-coordinate molybdenum sites are omitted.

μ_6-S bridging interactions contribute to stability. Remarkably, the latter cluster is actually $[Co_8(\mu_3\text{-NPh})_6(\mu_2\text{-NPh})_3(PPh_3)_2]^{4-}$ and contains six planar $Co(\mu_3\text{-NPh})_2(\mu_2\text{-NPh})$ units. This pattern of bridging ligands and approximately planar three-coordinate sites (excluding bonded metal atoms) is exactly what is found in FeMoco.

We seek synthetic routes to the clusters of nitrogenase. One approach to FeMoco has utilized sulfide-bridged oxidized $[MoFe_3S_4]^{3+}$ cubane-type clusters with total core content ($[Mo_2Fe_6S_9]^{4+}$) compositionally related to that of the cofactor ($MoFe_7S_9$).[13,14] A second approach involves reduced $[MoFe_3S_4]^{2+}$ clusters, which are obtained by the reaction of oxidized clusters with tertiary phosphines.[15,16] This approach is based on the conclusions that four or more iron atoms of FeMoco in the as-isolated form of nitrogenase are Fe(II),[17,18] and on the consistency of the ^{57}Fe isomer shift with an all-ferrous P^N state of the P-cluster.[19] The edge-bridged double cubane cluster $[(Cl_4cat)_2Mo_2Fe_6S_8(PEt_3)_6]$ has been prepared by the phosphine reduction method and structurally characterized.[15,16] We have shown that it is a synthetic precursor to the high-nuclearity species $[(Cl_4cat)_6(Et_3P)_6Mo_6Fe_{20}S_{30}]^{8-}$,[20] whose core structure is depicted in Figure 2. This cluster contains two identical fragments topologically related to the P-cluster. In the present investigation, we have further examined the reactivity of $[(Cl_4cat)_2Mo_2Fe_6S_8(PEt_3)_6]$, which contains two $[MoFe_3S_4]^{2+}$ cubane-type units. Several new reduced clusters have been isolated, among them one that contains an analogue of the P-cluster topology in a molecule of less complexity. The synthetic and structural results of that investigation are described here.

(11) Krüger, T.; Krebs, B.; Henkel, G. *Angew. Chem., Int. Ed. Engl.* **1989**, *28*, 61−62.
(12) Link, H.; Fenske, D. *Z. Anorg. Allg.Chem.* **1999**, *625*, 1878−1884.
(13) Huang, J.; Mukerjee, S.; Segal, B. M.; Akashi, H.; Zhou, J.; Holm, R. H. *J. Am. Chem. Soc.* **1997**, *119*, 8662−8674.
(14) Huang, J.; Holm, R. H. *Inorg. Chem.* **1998**, *37*, 2247−2254.
(15) Demadis, K. D.; Campana, C. F.; Coucouvanis, D. *J. Am. Chem. Soc.* **1995**, *117*, 7832−7833.
(16) Osterloh, F.; Segal, B. M.; Achim, C.; Holm, R. H. *Inorg. Chem.* **2000**, *39*, 980−989.
(17) Lee, H.-I.; Hales, B. J.; Hoffman, B. M. *J. Am. Chem. Soc.* **1997**, *119*, 11395−11400.
(18) Yoo, S. J.; Angove, H. C.; Papaefthymiou, V.; Burgess, B. K.; Münck, E. *J. Am. Chem. Soc.* **2000**, *122*, 4926−4936.
(19) McLean, P. A.; Papaefthymiou, V.; Orme-Johnson, W. H.; Münck, E. *J. Biol. Chem.* **1987**, *262*, 12900−12903; Yoo, S. J.; Angove, H. C.; Burgess, B. K.; Hendrich, M.. P.; Münck, E. *J. Am. Chem. Soc.* **1999**, *121*, 2534−2545.
(20) Osterloh, F.; Sanakis, Y.; Staples, R. J.; Münck, E., Holm, R. H. *Angew. Chem., Int. Ed. Engl.* **1999**, *38*, 2066−2070.

Experimental Section

Preparation of Compounds. All metathesis operations were carried out at room temperature in dried and degassed solvents under a pure dinitrogen atmosphere using Schlenk and glovebox techniques. $(Et_4N)(SH)$ (Alfa Aesar) was recrystallized from acetonitrile/ether prior to use, and 18-crown-6 (Aldrich) was washed with acetonitrile and dried in vacuo. $(Ph_3PMe)(BF_4)$ was prepared by metathesis of $(Ph_3PMe)Br$ and $NaBF_4$ in water and was obtained as colorless needles after crystallization from hot ethanol and drying in vacuo.

$(Et_4N)[(Cl_4cat)_2Mo_2Fe_6S_8(PEt_3)_6]$. A solution of $[K(18\text{-crown-6})](C_{14}H_{10})$ was prepared by stirring a mixture of 11 mg (0.28 mmol) of potassium and 65 mg (0.36 mmol) of anthracene in 4 mL of THF. After the potassium was completely dissolved (3 h), the solution was filtered through Celite and a solution of 73 mg (0.28 mmol) of 18-crown-6 was added with stirring. After 1 min, this solution was added dropwise over 4 min to a stirred suspension of 548 mg (0.28 mmol) of $[(Cl_4cat)_2Mo_2Fe_6S_8(PEt_3)_6]$[16] in 2 mL of THF. The solid dissolved followed by precipitation of a black solid upon stirring overnight. The solid was collected by filtration, suspended in 5 mL of THF, centrifuged, and dried in vacuo to give the $[K(18\text{-crown-6})]^+$ salt of the product cluster as 550 mg (85%) of a black solid. This material was dissolved in 5 mL of acetonitrile and the solution was filtered. A solution of 1.0 g (3.6 mmol) of $(Et_4N)(PF_6)$ in 4 mL of acetonitrile was added with stirring. The resulting solution was allowed to stand overnight, during which flat black rhomb-like crystals separated. The solid was collected by filtration, washed with acetonitrile (3 × 4 mL) and ether (2 × 5 mL) and dried in vacuo to afford the product as 262 mg (49%) of a black crystalline solid. Absorption spectrum (acetonitrile): λ_{max} (ϵ_M) 308 (sh, 48000) nm. Anal. Calcd. for $C_{56}H_{110}Cl_8Fe_6Mo_2NO_4P_6S_8$: C, 31.81; H, 5.24; Fe, 15.85; Mo, 9.07; N, 0.66; P, 8.79; S, 12.13. Found: C, 31.60; H, 5.29; Fe, 15.74; Mo, 9.16; N, 0.58; P, 8.80; S 12.17.

$(Ph_3PMe)_5[(Cl_4cat)_2(Et_3P)_4Mo_4Fe_{12}S_{20}K_3(DMF)]$. A solution of 69 mg (0.42 mmol) of $(Et_4N)(SH)$ in 1 mL of acetonitrile was added dropwise with stirring to a suspension of 416 mg (0.210 mmol) of $[(Cl_4cat)_2Mo_2Fe_6S_8(PEt_3)_6]$ in 3 mL of THF. After 1 min, the stirred brown-black reaction mixture was treated over 3 min with a solution of $K(C_{14}H_{10})$ prepared from 16.4 mg (0.419 mmol) of potassium and 90 mg (0.51 mmol) of anthracene in 4 mL of THF. The mixture was stirred for 3 d, during which a black crystalline solid separated. The solid was collected by centrifugation, washed with 5 mL of THF, and dried in vacuo to give 257 mg of the Et_4N^+ salt of the product cluster (without DMF). ^{1}H NMR (CD_3CN, anion): δ 1.97 (CH_3); 5.30, 6.89 (CH_2). The solid was dissolved in 10 mL of acetonitrile and the solution was filtered. A solution of 500 mg (1.37 mmol) of $(Ph_3PMe)(BF_4)$ in 10 mL of acetonitrile was added with stirring to the filtrate. The black precipitate was collected by filtration and dried in vacuo to yield 270 mg. The solid was dissolved in a minimal volume of DMF (ca. 1.0 mL) and 50 mg of solid $(Ph_3PMe)(BF_4)$ was added with stirring. Ether was diffused into the reaction mixture over 3 d, affording the product as black rhomb-like crystals. The solid was collected by filtration, washed with 5 mL of acetonitrile followed by 5 mL of ether. Drying in vacuo afforded the product as 125 mg (25%) of a black microcrystalline solid. Absorption spectrum (DMF): 316 (sh, 92000) nm. ^{1}H NMR (CD_3CN, anion): δ 1.99 (CH_3); 5.44, 6.93 (CH_2). Elemental analysis cannot distinguish between formulations containing one DMF (found to be coordinated in the crystal structure) and no DMF present. The calculated composition of the mono-DMF formulation is given. Anal. Calcd. for $C_{146}H_{157}Cl_{16}Fe_{12}K_3Mo_4NO_9P_9S_{20}$: C, 37.09; H, 3.35; Fe, 14.17; Mo, 8.12; N, 0.30; P, 5.90; S, 13.56. Found: C, 36.31; H, 3.57; Fe, 12.96; Mo, 8.11; N. 0.0; P, 6.38; S, 13.10.

In the sections which follow, clusters are designated as in the Chart. Here, ligands bound to molybdenum precede Mo; Cl_4cat = tetrachlorocatecholate(2−).

X-ray Structure Determinations. Crystal structures were obtained for the three compounds listed in Table 1. Black crystals of (Et_4N)[**2**] were grown by diffusion of an acetonitrile solution of $[K(18\text{-crown-6})]$[**2**] into a solution of $(Et_4N)(PF_6)$ in acetonitrile. A black polyhedral block was coated with Paratone oil and glued to a glass fiber with Apiezon L grease. The crystal was transferred to a Siemens SMART diffractometer equipped with an LT-2 low-temperature apparatus, and

Chart 1

$[(Cl_4cat)_2(Et_3P)_2Mo_2Fe_6S_8(PEt_3)_4]$	**1**[15,16]
$[(Cl_4cat)_2(Et_3P)_2Mo_2Fe_6S_8(PEt_3)_4]^{1-}$	**2**
$[(Cl_4cat)_4(Et_3P)_4Mo_4Fe_{12}S_{20}K_3(DMF)]^{5-}$	**3**
$[(Cl_4cat)_6(Et_3P)_6Mo_6Fe_{20}S_{30}]^{8-}$	**4**[20]
$[(Cl_4cat)_2(Et_3P)_2Mo_2Fe_6S_8(PEt_3)_4]^{4-}$	**5**

cooled in a dinitrogen stream to −60 °C. A total of 1271 frames was collected using ω-scans of 0.3°/frame, such that a hemisphere with maximum resolution of 0.75 Å was measured. The first 50 frames were recollected at the end of the data collection to monitor decay. None of the crystals showed decay during data collection. Cell parameters were retrieved using SMART software which corrects for Lorentz polarization; an absorption correction was applied using SADABS. The structure was solved by direct methods using the SHELXS-97 program suite and refined by least-squares methods on F^2 employing SHELXL-97. The compound crystallizes in monoclinic space group $P2_1/n$ with $Z = 4$. The asymmetric unit consists of one cation and one anion. All non-hydrogen atoms were refined anisotropically. Hydrogen atom positions were calculated and the atoms refined using a riding model with thermal ellipsoids 1.2 times those of bonded carbon atoms.

Black crystals of $(Ph_3PMe)_5$[**3**]·4.5DMF·0.5Et_2O were obtained from the preparative reaction mixture. Structure analysis was performed as for (Et_4N)[**2**]. The compound crystallizes in monoclinic space group $P2_1/n$ with $Z = 4$. The asymmetric unit contains one anion and five cations. Positions for one ether and five DMF molecules were also identified in the asymmetric unit but the occupancy of the ether molecule (atoms O1Q, C1Q, C2Q, C3Q, C4Q) and one of the DMF molecules (O1Y, N1Y, C1Y, C2Y, C3Y) was refined to 50%. Thus, this compound is formulated as $(Ph_3PMe)_5$[**3**]·4.5DMF·0.5Et_2O. All non-hydrogen atoms were refined anisotropically except those of the disordered solvate molecules. Black crystals of $(Et_4N)_4$[**5**]·3[**1**]·2Et_2O·2MeCN were obtained from the preparative reaction mixture (see text). These crystals occur in triclinic space group $P\bar{1}$ with $Z = 1$. The asymmetric unit consists of four halves of four independent clusters, two cations, one ether, and one acetonitrile solvate molecules. Based on the known metric features of **1**,[15,16] three clusters were assigned as neutral **1**, and the fourth cluster was tentatively assigned a 4- charge. All non-hydrogen atoms were refined anisotropically except those of the disordered ether solvate. Crystallographic data are contained in Table 1. (See paragraph at the end of the article for available Supporting Information.)

Other Physical Measurements. All measurements were made under strictly anaerobic conditions. ^{1}H NMR spectra were recorded with Bruker AM 300/400 spectrometers. Absorption spectra were obtained with Varian Cary 50 Bio spectrophotometer. Electrochemical measurements were made with a PAR Model 263 potentiostat/galvanostat using a Pt working electrode, 0.1 M $(Bu_4N)(PF_6)$ supporting electrolyte, and a SCE reference. Mössbauer spectra were collected with a constant acceleration spectrometer. Data were analyzed using WMOSS software (WEB Research Co., Edina, MN); isomer shifts are referenced to iron metal at room temperature.

Results and Discussion

Synthesis and Structures of Clusters. As may be seen from Figures 1 and 3, the cores of FeMoco and the P-cluster and the core of **1** have proximate structural relationships. The cofactor cluster consists of cuboidal $MoFe_3S_3$ and Fe_4S_3 units linked by three μ_2-S atoms to give a $MoFe_7S_9$ core of idealized C_{3v} symmetry. The P-cluster in the P^N state implicates two cuboidal Fe_4S_3 units bridged by two μ_2-S·Cys and one μ_6-S atom(s) in an Fe_8S_9 core of idealized C_{2v} symmetry. In this context, centrosymmetric **1** may be viewed as two cuboidal $MoFe_3S_3$ units linked by two μ_4-S atoms. Addition of sulfur to the $Mo_2Fe_6S_8$ core of **1** with accompanying rearrangement could afford clusters compositionally and structurally related to the native clusters of nitrogenase. As recently demonstrated, cluster **1** reacts with two equivalents of hydrosulfide in acetonitrile to afford polynuclear **4** (Figure 2), which is composed of a central $Mo_2Fe_8S_{12}$ and upper and lower $Mo_2Fe_6S_9$ fragments. The appearance of two P-cluster-like $Mo_2Fe_6S_9$ motifs in this cluster is possibly connected to the predominant ferrous character of precursor **1**. It is also apparent that **4** is not merely the product of sulfur addition to **1**, but rather it is a thermodynamically favored product in a complex reaction system which generates intermediate cluster species that assemble **4** by means of sulfide bridging. In an attempt to reduce the complexity of the reaction system and to arrive at a simpler product, we have further examined the reactivity of cluster **1** with hydrosulfide, here under reducing conditions. Regioselective addition of sulfide to a sufficiently reduced cluster of $Mo_2Fe_6S_8$ composition would, we hoped, proceed cleanly and afford the desired $Mo_2Fe_6S_9$ fragment in molecular form. This rationale gains some support from the findings, noted above, that nitrogenase cluster cores are mainly ferrous in character. Transformations of double cubane cluster **1** carried out in this work are summarized in Figure 3.

(a) $[(Cl_4cat)_2(Et_3P)_2Mo_2Fe_6S_8(PEt_3)_4]^{1-}$. Cluster **1** undergoes a chemically reversible one-electron reduction at −0.77 V vs SCE in dichloromethane.[16] Because of possible reduction of the $[Mo_2Fe_6S_8]^{4+}$ core of **1** in the reactions investigated, isolation of the one-electron reduction product was pursued. Treatment of **1** with one equivalent of a potassium crown salt of anthracenide led to the separation within minutes of black noncrystalline [K(18-crown-6)][**2**] (85%). Because this compound was obtained in crystalline form only in a twinned modification, cation exchange with $(Et_4N)(PF_6)$ in acetonitrile was performed to produce crystalline black (Et_4N)[**2**] (49%), suitable for an X-ray structure analysis.

Upon further study of the reaction of **1** with hydrosulfide, we discovered a second pathway to reduced cluster **2**. When a suspension of **1** in acetonitrile is treated with two equivalents of $(Et_4N)(SH)$, a black solution is formed from which, upon slow evaporation of all volatiles, black rhombs of (Et_4N)[**2**]·3CH_3CN form in small but reproducible yield (20%). The compound was identified crystallographically (Table 1). It is found in monoclinic space group $C2/c$ with the cluster disordered on a crystallographic inversion center. The structure was refined to $R_1(wR_2) = 0.0599(0.1276)$ and GOF = 1.103. (Structural details are reported as Supporting Information.) The formation of this reduced cluster is likely due to a side reaction between sulfide and displaced phosphine to generate Et_3PS and electrons. Reducing equivalents were presumably developed by the formal reaction $Et_3P + S^{2-} \rightarrow Et_3PS + 2e^-$, in which the source of sulfide is hydrosulfide or cluster sulfide. The formation of reducing equivalents from trialkylphosphines and $MoFe_3S_4$ clusters has been observed earlier, and was exploited, for example, in the synthesis of **1**.[15,16]

The structure of the reduced cluster is presented in Figure 4. Cluster **2** retains the edge-bridged topology of **1**[15,16] and other clusters such as $[Fe_8S_8(PCy_3)_6]$.[21] Interatomic distances in Table 2 are tabulated such that bonds equivalent under idealized C_2 symmetry are on the same line. In this way, it becomes immediately evident that there are certain significant metric differences between the two $MoFe_3S_4$ halves of the molecule. In particular, individual Fe−Fe separations and their mean values, 2.563(9) Å and 2.64(2) Å, are significantly different. Further, pairs of distances involving the μ_4-S(4,4a) atoms show large deviations. Differences between the bonds Fe(2)−S(4)/

(21) Goh, C.; Segal, B. M.; Huang, J.; Long, J. R.; Holm, R. H. *J. Am. Chem. Soc.* **1996**, *118*, 11844−11853.

Table 1. Crystallographic Data for Clusters [a]

	(Et_4N)[**2**][d]	$(Ph_3PMe)_5$[**3**]·4.5DMF·0.5Et_2O	$(Et_4N)_4$[**5**]·3[**1**]·2Et_2O·2CH_3CN[e]
formula	$C_{56}H_{110}Cl_8Fe_6Mo_2NO_4P_6S_8$	$C_{161.5}H_{193.5}Cl_{16}Fe_{12}K_3Mo_4N_{5.5}O_{14}P_9S_{20}$	$C_{232}H_{456}Cl_{32}Fe_{24}Mo_8N_6O_{17}P_{24}S_{32}$
Fw, g·mol^{-1}	2114.33	5094.11	8613.55
crystal system	monoclinic	monoclinic	triclinic
space group	$P2_1/n$	$P2_1/n$	$P\bar{1}$
Z	4	4	1
a, Å	15.8681(3)	19.644(4)	13.310(3)
b, Å	24.7648(3)	20.548(4)	23.690(5)
c, Å	23.7240(4)	51.40(1)	31.330(6)
α, deg			102.81(3)
β, deg	109.464(1)	91.33(3)	98.81(3)
γ, deg			92.83(3)
V, Å^3	8790.0(2)	20739(7)	9484(3)
d_{calc}, g·cm^{-3}	1.598	1.631	1.508
μ, mm^{-1}	1.818	1.635	1.687
T, K	213	213	213
θ range, deg	1.23−27.50	1.43 − 27.00	0.88−27.50
GOF (F^2)	0.987	1.010	1.086
R_1[b], wR_2[c]	0.0470, 0.0999	0.0573, 0.1055	0.0579, 0.1465

[a] Collected using Mo Kα ($\lambda = 0.71073$ Å) radiation. [b] $R_1 = \sum||F_o| - |F_c||/\sum|F_o|$. [c] $wR_2 = \{\sum[w(F_o^2 - F_c^2)^2]/\sum[w(F_o^2)^2]\}^{1/2}$. [d] Also obtained as (Et_4N)[**2**]·3CH_3CN in monoclinic space group $C2/c$, $a = 35.447(6)$, $b = 19.470(2)$, $c = 14.284(2)$ Å, $\beta = 101.36(2)°$, V = 9665(2) Å^3, Z = 4. [e] Oxidation state assignment for individual clusters in $(Et_4N)_4$[**5**]·3[**1**]·2Et_2O·2CH_3CN is tentative (see text).

Fe(3a)−S(4a) and Fe(3)−S(4)/Fe(2a)−S(4a) are 0.086 and 0.084 Å, respectively. The remainder of the core distances (Mo−Fe, Mo−S, other Fe−S) are largely unaffected. Corresponding Fe−μ_4-S(4,4a)−Fe angles differ by 2.1−5.2°. In a previous comparison of average core dimensions of $[MoFe_3S_4]^{3+,2+}$ clusters,[16] it was observed that, for reasons not yet clear, reduced clusters have the shorter Fe−Fe distances. The mean value in the triclinic centrosymmetric form of **1** is 2.62(2) Å (range 2.610(8)−2.641(8) Å).[16] We conclude that cluster **2** exhibits an unsymmetrical electron distribution in its crystalline Et_4N^+ salt. If the Fe−Fe distance trend continues, $[MoFe_3S_4]^{2+}$ and $[MoFe_3S_4]^{1+}$ units are associated with the longer and shorter Fe−Fe distances, respectively. In (Et_4N)[**2**]·3CH_3CN, disorder leads to indistinguishable $[MoFe_3S_4]^{2+,1+}$ units.

(b) $[(Cl_4cat)_4(Et_3P)_4Mo_4Fe_{12}S_{20}K_3(DMF)]^{5-}$. A variation on the preceding two methods for the synthesis of **2** was explored. When the treatment of **1** with 1−4 equivalents of potassium anthracenide in THF is followed by addition of a solution of two equivalents of $(Et_4N)(SH)$ in acetonitrile, a new isolable cluster species is produced. Cluster **3** separates as the Et_4N^+ salt when the reaction mixture is stirred at ambient temperature for 3 days; best yields were obtained with two equivalents of anthracenide. Cation exchange with $(Ph_3PMe)(BF_4)$ in acetonitrile followed by crystallization from DMF/ether produces crystals of $(Ph_3PMe)_5$[**3**]·0.5Et_2O·4.5DMF, suitable for an X-ray structure determination. In **3**, whose structure is discussed below, two $Mo_2Fe_6S_9$ units of the type previously observed in **4** are directly linked to each other through two sulfide atoms. Three potassium ions from the reductant are intercalated into the Mo−Fe−S framework. From ^{57}Fe isomer shifts, we have proposed the description $[Mo^{3+}Fe^{2+}{}_2Fe^{3+}]$ for each unit in **1**.[16] If the Mo^{3+} designation is retained, the description $[Mo^{3+}{}_2Fe^{2+}{}_4Fe^{3+}{}_2]$ follows for the fragments of **3**, excluding the possibility of protonated sulfide in the core. It thus appears that **3** is not reduced relative to **1**, and that the role of potassium anthracenide is merely to provide the potassium ions needed to "glue" together two $Mo_2Fe_6S_9$ units and reduce the overall charge of the cluster in a medium of low dielectric constant. As established by a control experiment, however, **3** does not form when potassium anthracenide in the reaction with **1** is replaced by KPF_6 as a potential source of potassium ions. It is therefore likely that, although the final product of the reaction between **1**, hydrosulfide, and $KC_{14}H_{10}$ is not the electron-sink in the system, reduced precursors must play a necessary (but presently unknown) role in its formation.

The structure of cluster **3** is presented in Figure 5; a stereoview is provided in Figure 6. Except for those involving potassium ions, the bond lengths in Table 3 are mean values of individual distances related by the mirror plane specified in Figure 5. No crystallographic symmetry is imposed on the cluster, which contains two $Mo_2Fe_6S_9$ fragments of the type previously encountered in **4**.[20] These fragments have idealized C_s symmetry, are isostructural and essentially isometric, and are most notable for their central μ_6-S(9,9A) atoms each of which bridges two cuboidal $MoFe_3(\mu_3\text{-}S)_3$ units. In each fragment, the iron atoms are present in distorted tetrahedral FeS_4 coordination units. In the course of the formation of **3** from **1**, phosphine ligands are displaced from the iron sites but the single phosphine at each molybdenum site is retained in distorted octahedral MoO_2PS_3 coordination. The two fragments are connected by two μ_2-S(10,11) atoms to form an Fe_4S_4 ring whose atoms S(9,9A) bind the central ion K(1). This ion shows eight K−S interactions in the range 3.23−3.60 Å. Ions K(2) and K(3) are held in the structure by seven or eight interactions with chlorine, oxygen, and sulfur atoms at 2.82−3.56 Å. Ion K(2) binds one DMF molecule at a K−O distance of 2.680(6) Å. In the context of alkali metal ion binding by chalcogenide clusters, **3** resembles $[Na_9Fe_{20}Se_{38}]^{9-}$, in which nine sodium ions are retained within a cyclic cluster framework.[22] Despite their somewhat different coordination environments, the $Mo_2Fe_6S_9$ units in **3** are isostructural with the respective units in **4**. The only notable exception is a difference in the mean Fe(6)−S(9)−Fe(3) angles for **3** (138.9(1)°) and the corresponding angle in **4** (145.3(2)°), which suggests that the $Mo_2Fe_6S_9$ fragments are most flexible around the central μ_6-S bridge. Other bond distances and angles are unexceptional compared to those of **4**. The structures of **3** and the nitrogenase P-cluster are compared below.

Mössbauer Spectra. We have collected spectra of four samples of cluster **2** with Et_4N^+ or K(18-crown-6)$^+$ counterions. The 4.2 K Mössbauer spectra of polycrystalline samples exhibit broad magnetic features indicating that cluster **2** has a paramagnetic ground state and that the spin relaxation is

(22) You, J.-F.; Papaefthymiou, G. C.; Holm, R. H. *J. Am. Chem. Soc.* **1992**, *114*, 2697−2710.

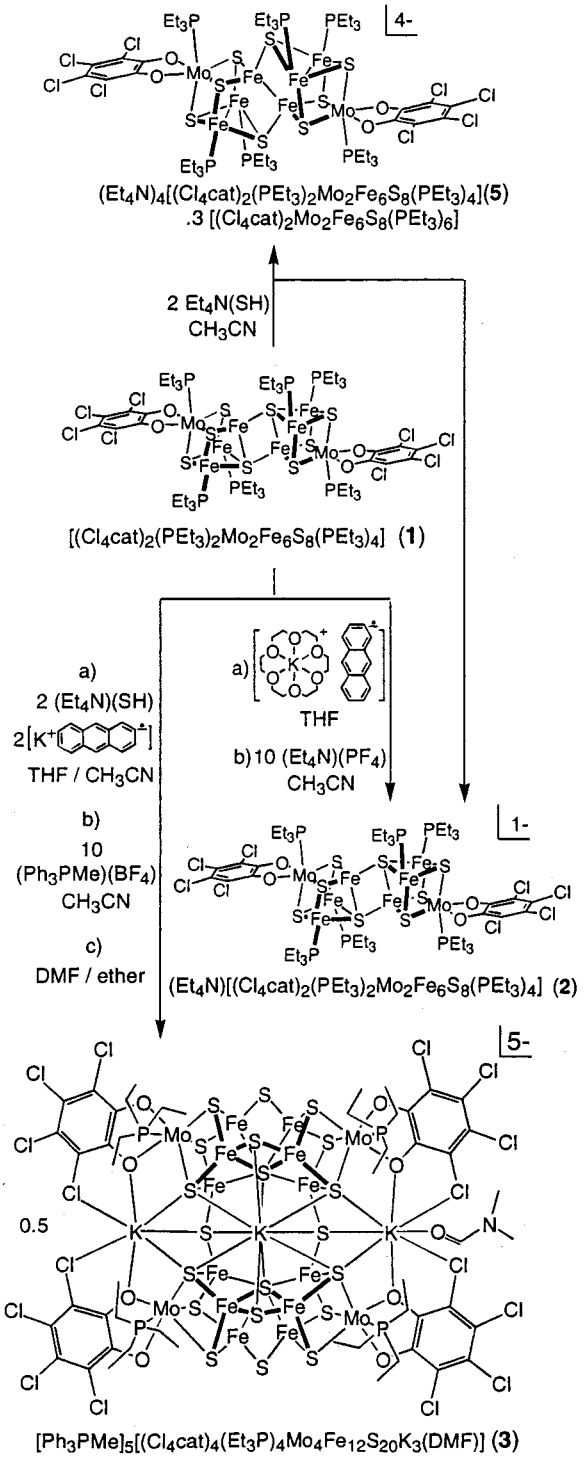

Figure 3. Scheme for the formation of clusters **2**, **3**, and **5** derived from double cubane cluster **1** under the indicated conditions. Oxidation state assignment for individual clusters in $(Et_4N)_4$[**5**]·3[**1**]·$2Et_2O$·$2CH_3CN$ is tentative (see text).

intermediate. At temperatures above 100 K, Mössbauer spectra of all samples of **2** take the appearance of a broad, asymmetric quadrupole doublet.[23] The average isomer shift of the doublet

(23) We note that at room temperature the differences in the Mössbauer parameters for the three sites of cluster **1** which are visible at 4.2 K cannot be observed. This is due to the large temperature dependence of the quadrupole splitting of one of the sites. In the case of cluster **2**, intermediate relaxation prevents us from analyzing the spectra at temperatures below room temperature and from obtaining information about possible differences between local sites of the $[MoFe_3S_4]$ cores.

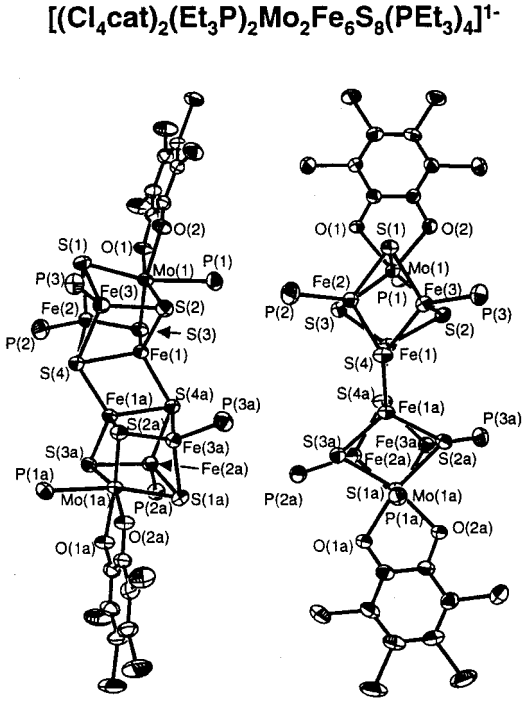

Figure 4. Two views of the structure of cluster **2** parallel (left) and perpendicular (right) to the bridging Fe(1,1a)S(4,4a) rhomb, showing 50% probability ellipsoids and the atom labeling scheme. Atoms labeled (n) and (na) are equivalent under idealized C_2 symmetry.

Table 2. Selected Interatomic Distances [Å] for Cluster **2**[a]

Mo(1)−Fe	2.66(1)[a]	Mo(1a)−Fe	2.67(1)[b]
Fe(1)−Fe(2)	2.5551(9)	Fe(1A)−Fe(2a)	2.6494(9)
Fe(1)−Fe(3)	2.5736(9)	Fe(1A)−Fe(3a)	2.6191(9)
Fe(2)−Fe(3)	2.5599(9)	Fe(2A)−Fe(3a)	2.6406(9)
	2.563(9)[b]		2.64(2)[b]
Mo(1)−S(1)	2.423(1)	Mo(1A)−S(1a)	2.434(1)
Mo(1)−S(2)	2.384(1)	Mo(1A)−S(2a)	2.354(1)
Mo(1)−S(3)	2.369(1)	Mo(1A)−S(3a)	2.366(1)
Fe(1)−S(4a)	2.289(1)	Fe(1A)−S(4)	2.234(1)
Fe(1)−S(4)	2.446 (1)	Fe(1A)−S(4a)	2.458(1)
Fe(2)−S(4)	2.378(1)	Fe(2A)−S(4a)	2.275(1)
Fe(3)−S(4)	2.359(1)	Fe(3A)−S(4a)	2.292(1)
Fe(1)−S(2)	2.280(1)	Fe(1A)−S(2a)	2.268(1)
Fe(1)−S(3)	2.265(1)	Fe(1A)−S(3a)	2.270(1)
Fe(2)−S(1)	2.266(1)	Fe(2A)−S(1a)	2.238(1)
Fe(2)−S(3)	2.254(1)	Fe(2A)−S(3a)	2.240(1)
Fe(3)−S(1)	2.264(1)	Fe(3A)−S(1a)	2.231(1)
Fe(3)−S(2)	2.247(1)	Fe(3A)−S(2a)	2.238(1)
	2.26(1)[c]		2.25(2)[c]
Fe(2)−P(2)	2.350(2)	Fe(2A)−P(2a)	2.313(1)
Fe(3)−P(3)	2.361(2)	Fe(3A)−P(3a)	2.328(2)
Mo(1)−P(1)	2.589(1)	Mo(1A)−P(1a)	2.578(1)
Mo(1)−O	2.115(9)[d]	Mo(1A)−O	2.114(4)[d]

[a] Atoms labeled (n) and (na) are related under idealized C_2 symmetry. [b] Mean of 3. [c] Mean of 6. [d] Mean of 2.

decreases from 0.50 mm/s at 100 K to 0.42 mm/s at room temperature, a variation typical for second-order Doppler shift. The line width of the quadrupole doublet decreases also with increasing temperature as a result of increased spin relaxation rate. At room temperature, the Mössbauer spectrum can be resolved in two quadrupole doublets as is evident in Figure 7B. The two possibilities for assigning these doublets are given in Table 4. Observation of two distinct quadrupole doublets indicates the presence of at least two types of iron and the 1:1 stoichiometry of the doublets suggests that each of them represents the iron sites in the $[MoFe_3S_4]^{2+}$ and $[MoFe_3S_4]^{1+}$

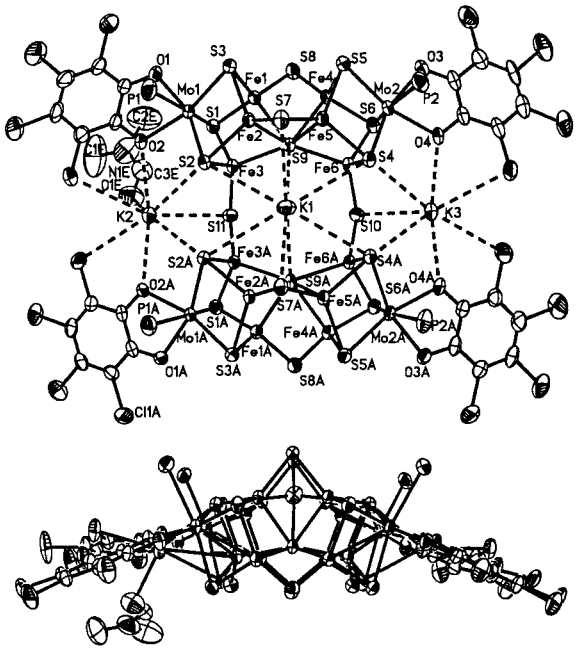

Figure 5. Frontal (upper) and edge (lower) views of cluster **3** showing 50% probability ellipsoids and the atom labeling scheme. Atoms labeled (n) and (nA) are related by a fictitious mirror plane between the two $Mo_2Fe_6S_9$ subunits.

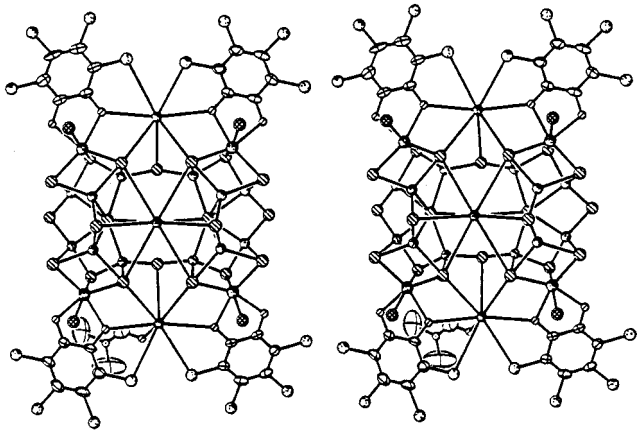

Figure 6. Frontal stereoview of cluster **3**.

units, respectively. One-electron oxidation of tetrahedral $Fe^{II}S_4$ species with thiolate or sulfide and thiolate ligands results in a decrease of ca. 0.45 mm/s in isomer shift. This leads to an estimate of ca. 0.15 mm/s decrease per iron site of a $[MoFe_3S_4]$ core. Analysis of the Mössbauer data for $[MoFe_3S_4]^z$ clusters reported in the literature indicates that a one-electron difference between the core oxidation states leads to differences in the cluster average isomer shift $\lesssim$0.12 mm/s. Therefore, assignment (a) in Table 4 is more likely correct. To test further the assignment, we have collected a room-temperature Mössbauer spectrum for cluster **1** (Figure 7A), which contains two $[MoFe_3S_4]^{2+}$ cores. This spectrum can be simulated by a single quadrupole doublet with $\delta = 0.37$ mm/s and $\Delta E_Q = 0.88$ mm/s. Assuming similar second-order Doppler shift and Debye−Waller factors for **1** and **2**, comparison of the isomer shifts indicates that the doublet with $\delta = 0.40$ mm/s in **2** represents the $[MoFe_3S_4]^{2+}$. These spectroscopic findings support the conclusion of the structural analysis that **2** has an unsymmetrical electron distribution. The difference in isomer shifts indicates that the reduction is substantially based on the iron atoms.

Table 3. Selected Interatomic Distances [Å] for Cluster **3**

Mo(1)−Fe(1)[a]	2.75(2)	Mo(2)−Fe(4)[a]	2.731(4)	K(1)−S(2)	3.506(2)
Mo(1)−Fe(2)	2.71(1)	Mo(2)−Fe(5)	2.7061(1)	K(1)−S(4)	3.476(2)
Mo(1)−Fe(3)	2.722(2)	Mo(2)−Fe(6)	2.704(2)	K(1)−S(7)	3.357(2)
				K(1)−S(9)	3.229(2)
Fe(1)−Fe(2)	2.71(2)	Fe(2)−Fe(5)	2.700(4)	K(1)−S(2A)	3.596(2)
Fe(1)−Fe(3)	2.77(2)	Fe(4)−Fe(5)	2.72(1)	K(1)−S(4A)	3.515(2)
Fe(1)−Fe(4)	2.76(3)	Fe(4)−Fe(6)	2.77(2)	K(1)−S(7A)	3.236(2)
Fe(2)−Fe(3)	2.81(3)	Fe(5)−Fe(6)	2.81(2)	K(1)−S(9A)	3.373(2)
Mo(1)−S(1)	2.400(3)	Mo(2)−S(6)	2.398(4)	K(2)−O(2)	2.818(4)
Mo(1)−S(2)	2.367(3)	Mo(2)−S(4)	2.369(4)	K(2)−S(2)	3.558(2)
Mo(1)−S(3)	2.35(1)	Mo(2)−S(5)	2.354(4)	K(2)−Cl(4)	3.294(2)
				K(2)−S(11)	3.258(2)
Fe(1)−S(9)	2.40(1)	Fe(4)−S(9)	2.42(2)	K(2)−O(2A)	2.876(4)
Fe(2)−S(9)	2.40(2)	Fe(5)−S(9)	2.43(3)	K(2)−S(2A)	3.398(2)
Fe(3)−S(9)	2.365(9)	Fe(6)−S(9)	2.35(2)	K(2)−Cl(4A)	3.298(2)
				K(2)−O(1E)	2.680(6)
Fe(1)−S(1)	2.235(3)	Fe(4)−S(5)	2.261(1)		
Fe(1)−S(3)	2.25(1)	Fe(4)−S(6)	2.243(7)	K(3)−O(4)	2.817(4)
Fe(1)−S(8)	2.208(4)	Fe(4)−S(8)	2.208(2)	K(3)−S(4)	3.386(2)
				K(3)−Cl(8)	3.300(2)
Fe(2)−S(2)	2.241(3)	Fe(5)−S(4)	2.2505(2)	K(3)−S(10)	3.223(2)
Fe(2)−S(3)	2.255(9)	Fe(5)−S(5)	2.266(3)	K(3)−O(4A)	2.816(4)
Fe(2)−S(7)	2.216(9)	Fe(5)−S(7)	2.219(7)	K(3)−S(4A)	3.299(2)
				K(3)−Cl(8A)	3.232(2)
Fe(3)−S(1)	2.257(6)	Fe(6)−S(4)	2.266(3)		
Fe(3)−S(2)	2.255(1)	Fe(6)−S(6)	2.257(1)		
Fe(3)−S(11)	2.198(8)	Fe(6)−S(10)	2.205(1)		
Mo(1)−P(1)	2.60(1)	Mo(2)−P(2)	2.60(1)		
Mo(1)−O(1)	2.13(1)	Mo(2)−O(3)	2.117(1)		
Mo(1)−O(2)	2.157(3)	Mo(2)−O(4)	2.153(4)		

[a] Mean values (see text and Figure 5).

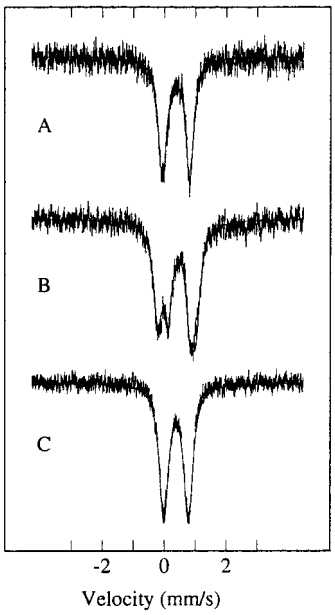

Figure 7. Zero-field Mössbauer spectra of polycrystalline **1** (A), **2** (B), and **3** (C) collected at room temperature. The solid lines drawn through the experimental data represent the sum of quadrupole doublets with parameters given in Table 4.

The Mössbauer spectra of **3** are represented by an asymmetric quadrupole doublet at all temperatures; the room temperature spectrum is shown in Figure 7C. The nearly identical isomer shifts of **1** and **3** support the proposition raised earlier that the iron population of **3** is not reduced relative to precursor **1**. Further, the Mössbauer parameters of **3** at 4.2 K are very close to those of **4** ($\delta = 0.52$ mm/s, $\Delta E_Q = 0.8$ mm/s at 4.2 K),[20] indicating that the two clusters have the same or very similar iron mean oxidation state.

Redox Properties. Clusters containing the cubane-type $MoFe_3S_4$ core generally exhibit one or two chemically reversible

Table 4. Zero-Field Mössbauer Parameters for Mo−Fe−S Clusters

compd	temp [K]		isomer shift[a] [mm/s]	quadrupole splitting[a] [mm/s]	fraction
1	4.2		0.48	0.93	70
			0.44	1.69	30
	300		0.37	0.88	100
2	300	(a)[b]	0.40	1.24	50
			0.47	0.72	50
		(b)[b]	0.31	1.04	50
			0.57	0.91	50
3	4.2		0.51	0.82	100
	300		0.38	0.79	100

[a] Typical precision for reported isomer shifts is ±0.02 mm/s and for quadrupole splittings is ±0.04 mm/s. [b] (a) and (b) are two possible line assignments.

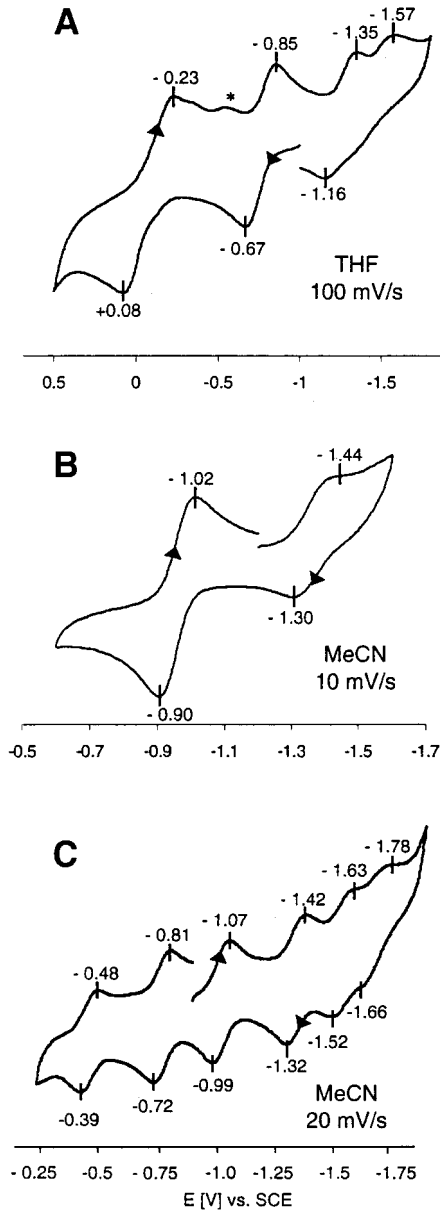

Figure 8. Cyclic voltammograms of clusters **2** (A), **3** (B), and **4** (C) under the indicated conditions; peak potentials vs SCE are indicated. *Product from oxidation at +0.08 V.

redox steps in cyclic voltammetry encompassing the oxidation levels $[MoFe_3S_4]^{3+,2+,1+}$.[16] Cyclic voltammograms of **2**, **3**, and **4** are shown in Figure 8. In acetonitrile solution, **2** reveals irreversible oxidative behavior, probably because of the insolubility of the product **1**. In THF solution, **2** gives rise to two quasireversible oxidation process at −0.76 V and −0.07 V, which involve the core oxidation states $[Mo_2Fe_6S_8]^{5+/4+/3+}$. These are appropriate combinations of the three individual cubane oxidation states. Two poorly defined reductions are observed at more negative potentials, suggesting generation of $[Mo_2Fe_6S_8]^{2+,1+}$ species. The two quasireversible redox features of **2** in THF correspond to those of **1** in dichloromethane ($E_{1/2}$ = −0.06, −0.77 V), further confirming **2** as a monoanion. Cluster **3** in acetonitrile solution undergoes a reversible oxidation at −0.96 V corresponding to the couple $[Mo_4Fe_{12}S_{20}]^{1+/0}$ and an irreversible reduction at ca. −1.37 V. Cluster **4**, on the other hand, shows a remarkably extensive set of redox reactions in acetonitrile. Four reductions are observed at −1.01, −1.35, −1.56, and −1.69 V and two oxidations at −0.78 and −0.45 V. Differential pulse voltammetry reveals six features with roughly comparable areas in the interval −0.2 to −1.8 V, in agreement with six consecutive one-electron processes. Because of differences in charge and structure between **3** and **4**, the former does not convey the locus of any of the redox steps of **4** which, given the number of steps, must implicate both the central and terminal fragments. These observations imply access to (at least) the oxidation states $[Mo_2Fe_6S_9]^{3+,2+,1+}$ by redox reactions of a hypothetical μ_6-S double cubane such as $[(Cl_4cat)_2(Et_3P)_2Mo_2Fe_6S_9(PEt_3)_2]^{2-}$.

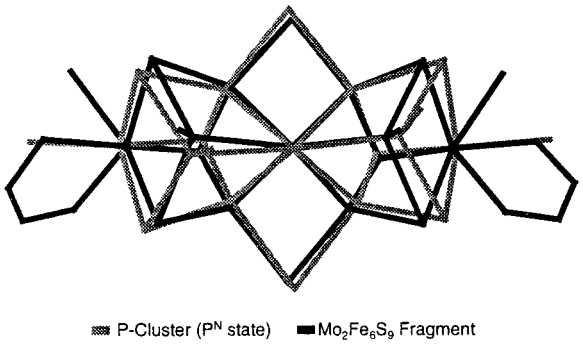

Figure 9. Best-fit superposition of the cores of a $Mo_2Fe_6S_9$ fragment of **3** and a P-cluster (P^N state) of *Klebsiella pneumoniae* MoFe protein.[3] Coordinates of the P-cluster were taken from the Brookhaven Protein Database (1QGU). The fragment containing Fe(1−6) and S(7) and the P-cluster coordinated by Cys α61,87,153 and Cys β68,93,151 were fitted using the subroutine OFIT of the SHELXS package.

Structural Comparison with P-Cluster. Examination of Figures 1 and 5/6 readily reveals the structural similarity of the $Mo_2Fe_6S_9$ fragments of **3** and the P-cluster in the P^N state. The former contains two $MoFe_3(\mu_3\text{-}S)_3$ and the latter two $Fe_4(\mu_3\text{-}S)_3$ fragments, both types of cuboidal geometry, bridged by a μ_6-S atom. The intra-fragment atoms μ_2-S(7,8) and μ_2-S(7A,8A) simulate cysteinate bridging, and the inter-fragment atoms S(10,11) two of the four terminal cysteinate ligands, in the P-cluster. In an obvious departure from the P-cluster, the fragments contain octahedral molybdenum sites in place of two Fe−S·Cys fragments. Provided in Figure 9 is a further comparison of the two structures in the form of a best-fit superposition of the 6Fe + μ_6-S set of atoms common to both. In the comparison, we have utilized the structure of the *Klebsiella pneumoniae* MoFe protein determined at 1.6 Å resolution.[3] Positional deviations vary from 0.145 Å (μ_6-S) to 0.315 Å (two iron atoms), with a weighted rms deviation of 0.229 Å. In **3**, the bond length order Fe−μ_6-S (2.39(6) Å) > Fe−μ_3-S (2.25(1) Å) > Fe−μ_2-S (2.213(6) Å), anticipated from other Fe−S cluster structures,[24,25] is clear. In the P-cluster, the trend Fe−μ_6-S (2.45(3) Å) > Fe−μ_3-S (2.31(4) Å) is discernible.

The Fe−μ_2-S·Cys bond lengths occur in the range 2.32(1)-2.47(2) Å, and are not strictly comparable to Fe−μ_2-S in **3** because of the ligand charge difference. In the P-cluster, iron−iron distances within the cuboidal units are rather variable, defining the range 2.52(3)−2.85(1) Å with the majority of values near the lower end. In cluster **3**, the variation is much less and the distances average to 2.77(4) Å. We note that the largest Fe−μ_6-S−Fe angles in the two structures are quite different. In **3**, the Fe(3)−S(9)−Fe(6) angle is 138.9(7)°, whereas in the P-clusters the corresponding mean angle is 157.6°. The cause of this difference is unclear. We have already observed that clusters of this type may be most flexible around the μ_6-S bridge atom. Strict congruence between the two structures is not realized and, given the probable influence of the protein, would not be expected. However, there is sufficient relationship in cluster overall shape, atom connectivity, and metric features to sustain the $Mo_2Fe_6S_9$ fragments as topological analogues of the P-cluster in the P^N state. While not as closely related to FeMoco, we note several relevant features of **3**. The cluster is a compositional analogue in terms of total metal and sulfur content and contains two cuboidal units bridged by three sulfide atoms, albeit with six tetrahedral instead of trigonal iron sites implicated in the bridges.

Another Structural Motif Derived from Cluster 1. On occasion, the mixed salt $(Et_4N)_4$[**5**]·3[**1**]·$2Et_2O$·2MeCN was obtained as a minor byproduct of the reaction between **1** and hydrosulfide. The material was obtained as polyhedral blocks and was crystallographically identified. The triclinic crystals contain two structurally distinct clusters in a 1:3 ratio, four cations, and four solvate molecules. Unambiguous charge assignment for individual clusters cannot be made using exclusively the present X-ray data but we favor the $(Et_4N)_4$[**5**]·3[**1**]·$2Et_2O$·2MeCN formulation for the following arguments. First, the structural parameters of the majority clusters are very similar to neutral cluster **1** identified in two previous structure determinations, suggesting neutral charges for these components. Second, the unique cluster **5** is at the center of gravity of four Et_4N^+ cations, whose charges need to be balanced by four negative cluster charges; cluster **5** is thus likely to have a charge of 4−.

The structure of **5** is set out in Figure 10 together with selected dimensions. The edge-bridged arrangement of initial cluster **1** has been transformed into a disulfido-bridged dimer of cuboidal $MoFe_3S_3$ units. The final structure may be visualized as resulting from the cleavage of the two intracubane Fe−S bonds in the bridging Fe_2S_2 rhomb of **1** to form μ_3-S(4,4a) from μ_4 atoms and the forging of a direct Fe(1)−Fe(1a) bond with length 2.408(2) Å. This results in a compression of the core along its longer axis, such that the Mo···Mo separation is 6.755 Å compared to 7.884 Å in **1**. Atoms Fe(1,1a) are now located in distorted trigonal S_3 environments with S−Fe−S angles of 109.71(8)°, 111.00(8)°, and 115.07(7)° and are displaced 0.64 Å from the S_3 planes toward each other. The Fe(2,2a)−Fe(3,3a) distances of 2.437(2) Å are also suggestive of metal−metal bonds. The Mo−S, Fe−S, and other Fe−Fe distances are similar to those in **1** and **2**. The latter distances in triclinic **1** are in the small range 2.610(8)−2.641(8) Å.[16] The unusual structure of **5** includes three Fe−Fe bonds formed by the apparent addition of four electrons to the core of **1** with accompanying rearrangement. This structure was included here to demonstrate another type of structural motif available by a transformation of **1**. We note the possibility of oxidative addition of sulfur to **5** to afford a compositional analogue $Mo_2Fe_6S_9$ of FeMoco.

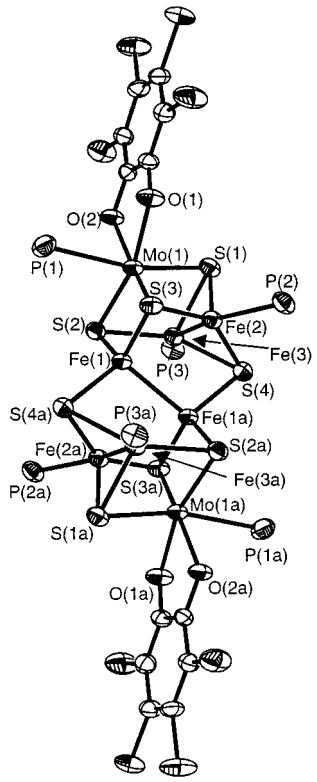

Figure 10. Structure of cluster **5** showing 50% probability ellipsoids and the atom labeling scheme. The cluster has a crystallographic inversion center. Selected bond distances (Å): Fe(1)−Fe(1a) 2.408(2), Fe(1)−Fe(2) 2.690(2), Fe(1)−Fe(3) 2.686(1), Fe(1)−Fe(2a) 2.774(1), Fe(1)−Fe(3a) 2.753(2), Fe(2)−Fe(3) 2.437(2), Mo−Fe 2.65(1) (mean), Mo−S 2.37(1) (mean), Fe−S 2.21(2) (mean).

Summary. The following are the principal results and conclusions of this investigation.

(1) The reaction system $[(Cl_4cat)_2Mo_2Fe_6S_8(PEt_3)_6]/K(C_{14}H_{10})$ in THF affords the reduced cluster $[(Cl_4cat)_2Mo_2Fe_6S_8(PEt_3)_6]^{1-}$, which retains the double cubane structure of its neutral precursor. As its crystalline Et_4N^+ salt, the cluster contains localized $[MoFe_3S_4]^{2+}/[MoFe_3S_4]^{1+}$ cubane-type units as deduced from the X-ray structure and Mössbauer spectroscopy. The reduced cluster is linked to its precursor by an oxidation step at −0.77 V in THF.

(2) The reaction system $[(Cl_4cat)_2Mo_2Fe_6S_8(PEt_3)_6]/2(Et_4N)(SH)/2K(C_{14}H_{10})$ in THF affords, after cation metathesis, the high-nuclearity cluster $[(Cl_4cat)_4(Et_3P)_4Mo_4Fe_{12}S_{20}K_3(DMF)]^{5-}$ as the Ph_3PMe^+ salt, which was identified crystallographically. The anthracenide reductant is required for product formation, although isomer shifts indicate that the average iron oxidation state in precursor and product clusters is unchanged.

(3) The structure of $[(Cl_4cat)_4(Et_3P)_4Mo_4Fe_{12}S_{20}K_3(DMF)]^{5-}$ consists of two isostructural $Mo_2Fe_6S_9$ fragments of idealized C_s symmetry connected by two Fe−μ_2-S−Fe bridges. In addition, three potassium ions are located between the clusters and interact with them to give the cluster additional stability. The fragments consist of $MoFe_3(\mu_3\text{-}S)_3$ cuboidal units bridged by a common μ_6-S atom and containing octahedral MoO_2PS_3 and tetrahedral FeS_4 coordination units. These fragments are isostructural with two such fragments present in the more complex cluster $[(Cl_4cat)_6(Et_3P)_6Mo_6Fe_{20}S_{30}]^{8-}$. Synthesis and electrochemical results indicate two oxidation states for the Mo_4

(24) Christou, G.; Sabat, M.; Ibers, J. A.; Holm, R. H. *Inorg. Chem.* **1982**, *21*, 3518−3526.
(25) Strasdeit, H.; Krebs, B.; Henkel, G. *Inorg. Chem.* **1984**, *23*, 1816−1825.

cluster and seven oxidation states for the Mo_6 cluster. In particular, the latter reveals four reductions and two oxidations over the interval -0.3 to -1.8 V in acetonitrile.

(4) On the basis of overall shape, atom connectivities, and metric parameters, the $Mo_2Fe_6S_9$ fragments in (3) are topological analogues of the P-cluster of nitrogenase in the reduced P^N state. These fragments and the $Na_2Fe_6S_9$ fragments in the cluster $[(Fe_6S_9(SMe)_2)_2Na_2]^{6-}$,[26] are currently the only synthetic entities possessing P-cluster topology.

(5) The synthetic procedure in (2) has achieved the goal of producing a cluster of lower nuclearity than $[(Cl_4cat)_6(Et_3P)_6Mo_6Fe_{20}S_{30}]^{8-}$ containing $Mo_2Fe_6S_9$ fragment(s).

(26) The disodium-bridged cluster $[(Fe_6S_9(SMe)_2)_2Na_2]^{6-}$ (ref 25) is a topological model of the P-cluster, with six iron and two sodium ions assuming the positions of the eight iron ions in the P-cluster. The Na···S and Na···Fe separations in the $Na_2Fe_6S_9$ fragments occur in the ranges 2.883−3.103 Å and 3.652−4.899 Å, respectively. These bonding parameters suggest that the sodium ions are only weakly coordinated.

The foregoing results and those presented earlier[20] demonstrate the utility of cluster **1** as a precursor to new structures resembling the P-clusters of nitrogenase. At present, three new cluster structural types (**3**, **4**, **5**) have been achieved in this laboratory by reactions of **1**, and several other types have been obtained by Coucouvanis and co-workers[9,10] under very different conditions. Among immediate goals are the synthesis of a cluster containing a single $Mo_2Fe_6S_9$ core unit and development of routes to Fe−S clusters structurally related to P-clusters. Research directed toward these goals is in progress.

Acknowledgment. This research was supported by NIH Grant GM 28856. F.O. is grateful to the Deutsche Forschungsgemeinschaft (DFG) for a postdoctoral fellowship.

Supporting Information Available: ORTEP representations and tables of crystallographic data for **2**, **3**, and **5**. Three X-ray crystallographic files in CIF format for the compounds in Table 1. This material is available free of charge via the Internet at http://pubs.acs.org.

IC000617H